Biosensors and Bioelectronics 96 (2017) 260–267

Contents lists available at ScienceDirect

Biosensors and Bioelectronics

journal homepage: www.elsevier.com/locate/bios

A label-free nanostructured plasmonic biosensor based on Blu-ray discs with integrated microfluidics for sensitive biodetection

Gerardo A. López-Muñoz[a,b], M.-Carmen Estevez[a,b,*], E. Cristina Peláez-Gutierrez[a,b], Antoni Homs-Corbera[a], M. Carmen García-Hernandez[c], J. Ignacio Imbaud[c], Laura M. Lechuga[a,b]

[a] Nanobiosensors and Bioanalytical Applications Group (NanoB2A), Catalan Institute of Nanoscience and Nanotechnology (ICN2), CSIC and the Barcelona Institute of Science and Technology, 08193 Bellaterra, Barcelona, Spain
[b] CIBER-BBN Networking Center on Bioengineering, Biomaterials and Nanomedicine, Spain
[c] Protein Alternatives, S.L., Tres Cantos, Madrid, Spain

ARTICLE INFO

Keywords:
Blu-ray disc
Plasmonic nanostructure
Integration
Microfluidics
Biosensing
Antibody

ABSTRACT

Nanostructure-based plasmonic biosensors have quickly positioned themselves as interesting candidates for the design of portable optical biosensor platforms considering the potential benefits they can offer in integration, miniaturization, multiplexing, and real-time label-free detection. We have developed a simple integrated nanoplasmonic sensor taking advantage of the periodic nanostructured array of commercial Blu-ray discs. Sensors with two gold film thicknesses (50 and 100 nm) were fabricated and optically characterized by varying the oblique-angle of the incident light in optical reflectance measurements. Contrary to the use normal light incidence previously reported with other optical discs, we observed an enhancement in sensitivity and a narrowing of the resonant linewidths as the light incidence angle was increased, which could be related to the generation of Fano resonant modes. The new sensors achieve a figure of merit (FOM) up to 35 RIU^{-1} and a competitive bulk limit of detection (LOD) of 6.3×10^{-6} RIU. These values significantly improve previously reported results obtained with normal light incidence reflectance measurements using similar structures. The sensor has been combined with versatile, simple, ease to-fabricate microfluidics. The integrated chip is only 1 cm^2 (including a PDMS flow cell with a 50 μm height microfluidic channel fabricated with double-sided adhesive tape) and all the optical components are mounted on a 10 cm×10 cm portable prototype, illustrating its facile miniaturization, integration and potential portability. Finally, to assess the label-free biosensing capability of the new sensor, we have evaluated the presence of specific antibodies against the GTF2b protein, a tumor-associate antigen (TAA) related to colorectal cancer. We have achieved a LOD in the pM order and have assessed the feasibility of directly measuring biological samples such as human serum.

1. Introduction

Nowadays there is increasing interest to develop portable point of care (POC) platforms in a cost-effective manner that provide fast and real-time responses and that meet clinical requirements in terms of sensitivity and specificity (Lopez et al., 2017). Optical biosensors based on Surface Plasmon Resonance (SPR) are promising platforms due to their sensitive performance and well-established surface functionalization protocols. In particular plasmonic biosensors using metallic nanostructures have undergone an extensive development because additional benefits in miniaturization and sensitivity can be achieved and can operate under low-complexity detection schemes (Estevez et al., 2014; Tokel et al., 2014). However, in order to achieve fully operative lab-on-a-chip (LOC) biosensor platforms several challenges need to be surpassed, such as promoting low-cost sensor fabrication techniques, incorporating effective microfluidics, increasing the throughput and implementing optical subsystems integration (Lopez et al., 2017). There have been some interesting approaches that try to solve these aspects, especially the integration of optics and microfluidics on chip. Although the biosensing capabilities with these examples are commonly demonstrated the devices require bulky detection schemes, which complicate POC integration (Acimovic et al., 2014; Malic et al., 2013). More integrated designs with reduced dimensions and simple instrumentation have been reported based on

* Corresponding author at: Nanobiosensors and Bioanalytical Applications Group (NanoB2A), Catalan Institute of Nanoscience and Nanotechnology (ICN2), CSIC and the Barcelona Institute of Science and Technology, 08193 Bellaterra, Barcelona, Spain; CIBER-BBN Networking Center on Bioengineering, Biomaterials and Nanomedicine, Spain.
E-mail address: mcarmen.estevez@icn2.cat (M.-C. Estevez).

http://dx.doi.org/10.1016/j.bios.2017.05.020
Received 3 March 2017; Received in revised form 3 May 2017; Accepted 9 May 2017
Available online 10 May 2017
0956-5663/

imaging systems. However most of them have limited sensitivity in the range of 10^{-5} RIU (Coskun et al., 2014; Cappi et al., 2015). Besides this, improving nanostructures design and performance to push sensitivity levels is currently under exhaustive research. During last years the development of novel fabrication methods and innovative nanostructures with promising performance have been reported (Kabashin et al., 2009; Lee et al., 2012; Gartia et al., 2013; Shen et al., 2013; Sreekanth et al., 2016). Nevertheless most of them still involve complex and expensive fabrication processes (Kooy et al., 2014; Seo et al., 2014; Chen, 2015), which limit their applicability outside the laboratory environment. A simple and cost-effective alternative fabrication method employs industrially produced patterned optical discs as a nanoslit-containing substrate to generate the SPR phenomena (Kaplan et al., 2009; Dou et al., 2012). This approach provides a high degree of controlled reproducibility while involving low-cost fabrication. In general, the bulk sensitivities obtained using optical discs as substrates (Dou et al., 2012) are similar to those obtained with engineered nanoslits (Lee et al., 2012, 2015) making them interesting for many applications, including biosensor devices development. The high availability of optical discs and their convenient standardized mass-production manufacturing processes make them especially attractive to build sensing platforms for POC devices.

Blu-ray discs in particular are top-down fabricated optical discs consisting of a polycarbonate substrate patterned with highly ordered concentric periodic nanoslits: 320 nm period, 160 nm width and approximately 20 nm depth (Kaplan et al., 2009; Dou et al., 2012). Obtaining plasmonic chips from Blu-ray discs involves a simple fabrication process, based on the coating of a metallic layer on the substrate. Recently the possibility to generate plasmonic effects in the visible range when incorporating metal layer films with thicknesses in the range of 50–100 nm (Dou et al., 2012; Guner et al., 2017) has been demonstrated. Blu-ray based chips present some advantages over other commercially available optical discs. They exhibit a plasmonic band in the visible region, whereas other optical discs present plasmonic bands in the near infrared spectra due to larger periods of the structures (Dou et al., 2012). This make Blu-ray discs a more interesting option, since near Infrared Radiation (IR) spectrometers commonly are more expensive, which can eventually increase the overall cost of a final device. Also, they traditionally possess lower resolution for the plasmonic detection compared with more convenient visible compact spectrometers. Moreover, the periodic nanostructures present in Blu-ray discs can promote the presence of Fano resonances (Luk'yanchuk et al., 2010). This is due to the coupling of the localized resonances in the nanoslits and the Wood´s anomalies present in high ordered nanostructures that behave as a grating (Offermans et al., 2011). This effect narrows the resonant linewidths and enhances the intensity of the optical fields.

Based on these considerations we present a simple, cost-effective nanostructured plasmonic biosensor based on Blu-ray discs with integrated microfluidics for high performance biosensing. The sensors were fabricated following extremely simple and reproducible processes. We considered two different metal layer thicknesses to evaluate its influence in the optical performance of the nanostructures. The chips were optically characterized under transverse-magnetic (TM) polarized white light at different angles of incidence to generate Fano resonant modes and to evaluate their performance as a biosensor platform. We used a wavelength shift interrogation method to optimize the biosensor performance by tuning the optical conditions and the thickness of the nanostructured substrate. We performed three-dimensional finite difference time-domain (FDTD) simulations to evaluate the reflectance spectra and the electric field distributions. With a view to achieve a compact operative device, further integration was done by incorporating a 1 cm^2 polydimethylsiloxane (PDMS) flow cell with a patterned microfluidics (single channel of 50 μm height) obtained using a simple and inexpensive double-sided adhesive tape. All the optical components are fixed on a 10×10 cm^2 portable prototype, illustrating its facile miniaturization, integration and potential portability. The viability of this configuration for biosensing was further explored by performing label-free measurements based on the detection of specific antibodies for GTF2b (general transcription factor IIB) protein, a tumor-associated antigen (TAA) related to colorectal cancer. We achieved a Limit of Detection (LOD) in the pM order. We also assessed the feasibility of measuring biological samples by evaluating diluted serum, achieving promising performance in this complex matrix.

2. Materials and methods

2.1. Fabrication and integration of the nanostructured plasmonic chip

Single layer recordable Blu-ray discs (TDK, T78088, Japan) were used after removal of their protective and reflective films. These were removed by trimming the disc around the edges and then by immersing it in a hydrochloric acid solution (1 M HCl) for 120 min. After consecutive rinsing with MilliQ water and ethanol and air drying of the substrate, gold layers up to 100 nm thickness were deposited by electron beam deposition (1 Å/s). Individual plasmonic chips (size of 1 cm^2) were obtained by cutting the gold-coated optical disc with a conventional computer numerical control (CNC) router (LPKF Laser & Electronics, Protomat C100/HF, Germany). The flow cell for carrying out real time measurements in solution was fabricated by patterning a microfluidic channel (10 mm length, 1 mm width, 50 μm height and 1 μL volume) using a cutting plotter (Graphtec America, Inc., CE6000-40, USA) in a 50 μm thick double-sided adhesive tape sheet (Nitto, D5331,Japan). A PDMS thin layer (2 mm thickness, Dow Corning Co., Sylgard 184, USA) was added as a cover to facilitate the connection of the fluidic tubes. The microchannel was designed to promote laminar flow and to increase the mass transfer near the sensor surface (See Fig. 1a).

2.2. Experimental setup and optical characterization

The integrated sensor chips were clamped to a custom-made optical platform (Fig. 1b). The chips were connected to a microfluidic system consisting of a syringe pump (New Era, NE-1000, USA), with adjustable pumping speed guaranteeing a constant liquid flow, and a manually operated injection valve (Valco Instruments Co. Inc., Cheminert C22-3186, USA). Reflectance measurements were performed under TM-polarization of a compact broadband light source (wavelength region between 360–2400 nm and approximately 9 mW output, HL-2000-HP Ocean Optics, US) at different incident angles (ranging from 30° to 70°). The incident excitation plane was perpendicularly aligned to the nanoslits direction. The reflected light was collected and fiber-coupled to a compact Charge-Coupled Device (CCD) spectrometer (Flame-T spectrometer, Ocean Optics, US). All optical components were mounted on a 10 cm×10 cm optical platform. Reflectivity spectra were acquired every 3 ms and 250 consecutive spectra were measured and averaged to provide the final spectrum. These acquisition parameters were considered appropriate to obtain optimum signal to noise (S/N) ratio without significantly increasing the data acquisition time. Real-time changes in the resonance peak position (λ_{SPP}) were tracked *via* polynomial fit by using virtual instrumentation software (National Instruments, Labview, USA). The bulk refractive index (RI) sensitivity and full width at half maximum (FWHM) of the sensor as a function of the incidence angle, were determined using solutions of glycerol in water (ranging from 4.2 mM to 136 mM, equivalent to a range of RIU between 1.3334 and 1.3463 RIU).

2.3. FDTD Simulations

Three-dimensional FDTD simulations were performed using commercial software (Lumerical Inc., FTDT solution, Canada). Structural parameters of the Blu-ray discs were used in the simulations (*i.e.* a slit

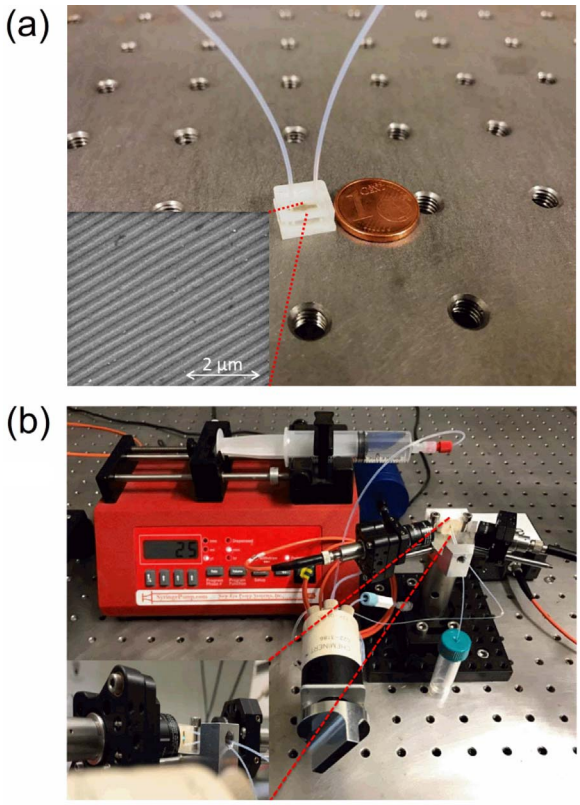

Fig. 1. Chip integration and experimental set-up. (a) Photography of the integrated chip with the microfluidics channel and a Scanning Electron Microscopy (SEM) image (insert) of the Blu-ray based plasmonic nanostructures. (b) Experimental set-up including the optical detection scheme and the microfluidic system.

period of 320 nm, slit width of 160 nm and a height of 20 nm). Periodic boundary conditions were used in x and y axis, and perfect matched layers (PML) approach was used in the z axis, with a uniform mesh size of 2 nm in all axis. The optical constants of the polycarbonate and gold were considered from Sultanova et al. (2009) and Johnson and Christy (1972), respectively, in the range from 400 nm to 1000 nm, under TM-polarized light with an oblique light incidence angle of 70°.

2.4. Surface functionalization with GTF2b and antibody detection assays

Alkanethiol for self-assembled monolayer (SAM) formation (16-mercaptohexadecanoic acid, MHDA), (1-ethyl-4 (3-dimethylaminopropyl) carbodiimide hydrochloride (EDC) and N-hydroxysulfosuccinimide (*s*-NHS) for carboxylic groups activation, ethanolamine and Tween 20 were acquired to Sigma–Aldrich (Germany). Poly(L-lysine)-graft-poly(ethylene glycol) co-polymer (PLL-PEG, MW~70000 $gmol^{-1}$) was purchased to SuSoS AG (Switzerland). Commercial serum was obtained from Sigma–Aldrich (Germany). Antibody anti-GTF2b was purchased to Santa Cruz Biotechnology (USA). GTF2b protein was produced in bacterial expression systems. The coding sequence of the DNA was cloned into pET28a(+) expression vector (Novagen) and transformed into protease deficient BL21(DE3) competent *E. coli* cells (Invitrogen). The protein was over-expressed in cultures of Luria Broth media (Pronadisa) containing kanamycin (Sigma-Aldrich) by inducing the strain with 0.8 nM of IPTG (Apollo Scientific Ltd). Bacterial pellets were then disrupted by sonication in buffer containing 20 mM sodium phosphate pH 7.4 (Merck), 500 mM NaCl, 0.5 mM EDTA, 1 mM DTT, 0.010g PMSF (Sigma-Aldrich), 1X Complete™ protease inhibitors (Roche), 0.25 mg/mL lysozyme (Sigma-Aldrich), 1% N-Lauroylsarcosine (Sigma-Aldrich) and 1% Triton X-100 (Sigma-Aldrich). The lysate was clarified by centrifugation and filtered through a 0.45 µm pore-size syringe filter (Sarstedt). The protein contained in the soluble fraction was purified by affinity chromatography (IMAC) using an ÄKTA FPLC system and HisTrap FF Crude columns (GE Healthcare). Purified GTF2b protein was eluted in PBS 1X, 0.1 M Arginine (Alfa Aesar), 150 mM Imidazole (Sigma-Aldrich), 1 mM DTT, 0.5 mM EDTA and 1X Complete™ protease inhibitor, pH 7.4. The protein was dialyzed in PBS 1X before use in the biosensing experiments.

Sensor chips (100 nm thickness gold layer) were cleaned and activated for surface functionalization by performing consecutive 1 min sonication cycles in ethanol and MilliQ water, drying with N_2 stream and finally by placing them in a UV/O_3 generator (BioForce Nanoscience, USA) for 30 min. GTF2b biofunctionalization and assay conditions for antibody detection were previously optimized and transferred to this biosensor (Soler et al., 2016). An alkanethiol SAM with reactive carboxylic groups was obtained by coating the sensor chip with 500 µM MHDA in ethanol overnight at room temperature. Then, the surface was rinsed with ethanol and dried with a N_2 stream. Prior to the biofunctionalization step, the chip was bonded to the microfluidics and placed in the optical platform. The immobilization of the GTF2b protein was performed *in situ*, and was continuously monitored in real time. For the activation of the carboxylic groups a solution of 0.2 M EDC/0.05 M s-NHS in MES buffer (100 mM pH 5.5) was injected and flowed over the SAM monolayer at 20 µL/min (using H_2O as running buffer). Subsequently, a 50 µg/mL GTF2b protein solution in PBS (10 mM pH 7.4) was injected and flowed at 5 µL/min. Finally, an ethanolamine solution (1 M pH 8.5) was injected for 2 min at 25 µL/min to block unreacted remaining active carboxylic groups. After immobilization, PBST 0.5% (PBS 10 mM pH 7.5+0.5% Tween 20) was settled as running buffer. For optimization and assessment studies, different concentrations of specific antibody diluted in PBST 0.5% were flowed over the functionalized surface at 25 µL/min. Regeneration of the surface was achieved by injecting 20 mM NaOH at 65 µL/min. Calibration curves were fitted to a one-site specific binding model. Data points for each concentration were collected after signal stabilization, around 900 s after injection. LOD and LOQ (Limit of Quantification) were calculated as the concentration corresponding to the blank signal plus three and ten times its standard deviation (SD), respectively. Specificity was confirmed by injecting a specific antibody for protein PIM1, which is another TAA also suspected to be related with colorectal cancer. For the evaluation in serum, an additional blocking step was considered according to previous results (Soler et al., 2016) based on the addition of a PLL-PEG solution (0.25 mg/mL) to minimize non-specific adsorptions.

3. Results and discussion

3.1. Characterization and simulation of nanostructured plasmonic sensor

Gold capped nanoslits were fabricated taking advantage of the precise and large area of nanostructured array present in commercial Blu-ray discs. Two gold film thicknesses (50 and 100 nm) were selected for the fabrication of the chips. These metallic film thicknesses were selected according to previous results (Dou et al., 2012; Guner et al., 2017). Dou et al. (2012) reported no significant differences in RI sensitivity for Blu-ray discs with metal layers thicknesses between 60 and 120 nm in reflection measurements at normal light incidence. On the other hand, simulations performed by Guner et al. (2017) showed that under 50 nm metal thickness layer, the plasmonic reflectance spectra lose sharpness due to the strong interaction of plasmonic wave with the underlying substrate. Above 100 nm of metal thickness no significant change in the plasmonic reflectance spectra is observed. In our case different angles of incident light (between 30° and 70°) were studied for the reflection measurements in order to evaluate its influence in the sensing performance due to the generation of other resonant modes under oblique-angle incident light. Optical characterization of the integrated sensors was performed under TM-polarized

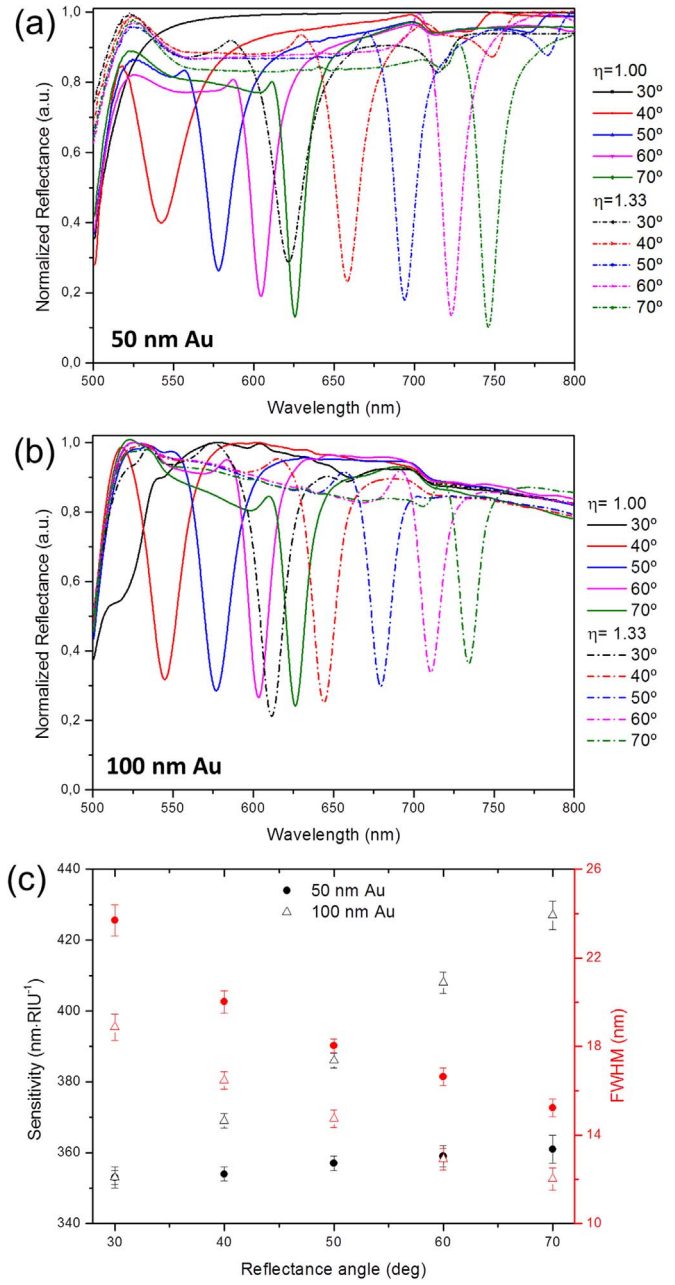

Fig. 2. Optical Characterization of the plasmonic chips. Variation of the reflectance spectra in air (η=1.00) and water (η=1.33) of nanostructured plasmonic chip with 50 nm (a) and 100 nm (b) gold layer thickness varying the oblique light incidence angle. (c) Variation of the bulk sensitivity (black) and FWHM linewidth (red) as function of the angle of the incidence light for the two gold thickness. (For interpretation of the references to color in this figure legend, the reader is referred to the web version of this article.)

broadband light. Reflection spectra were collected in air (η=1.00) and water (η=1.33).

Fig. 2a and b show the reflectance spectra for both thicknesses. First, a shift of λ_{SPP} to higher wavelengths is observed as the incidence angle increases. Also in both cases narrower resonant linewidths are observed, with a decrease in the FWHM. This behavior can be correlated with the possibility to induce Fano resonances in periodic nanoslits (Lee et al., 2015, 2016). These resonant modes narrow the resonant linewidths and enhance the intensity of the optical fields. This enhancement is due to the coupling of the localized resonances in the nanoslits and the Wood´s anomalies promoted by the high ordered periodic nanostructures of the Blu-ray discs that behave as a grating (Lee et al., 2016). The generation of the plasmonic effect for high order periodic nanostructures can be described by the Bloch wave surface plasmon polariton (BW-SPP), when the Bragg condition for one-dimensional periodic metallic structure is satisfied (Lee et al., 2015, 2016). Under oblique-angle incident light, it can be described by the following equation (Lee et al., 2016):

$$\lambda_{SPP} = \frac{P}{i}\left\{Re\left[\left(\frac{\varepsilon_m n^2}{\varepsilon_m + n^2}\right)^{1/2}\right] \pm \sin\theta\right\} \quad (1)$$

Where i is the resonant order, P is the period of the nanostructure, ε_m is the dielectric constant of the metal, n is the environmental refractive index and θ is the incident angle, respectively.

A red-shift in the resonant wavelength is expected when the RI of the medium near the gold surface increases. Also, for a given nanostructure period, the resonance wavelength is controlled by the light incident angle. The narrowing in the resonance peak with the increase in the incident angle is related to the interaction of the different resonance modes: Wood´s anomalies in periodic nanostructures, and the BW-SPP on the periodic surface. By increasing the incident angle, the BW-SPP at the metal/substrate interface interacts with the substrate modes (Lee et al., 2016). This interaction between different modes produces Fano resonances with narrower resonant linewidths (Lee et al., 2016; Xiao et al., 2015). Moreover, by increasing the angle of the incident light, the optical energy scattered from one nanostructure can be collected by neighboring nanostructures, decreasing radiative loss (Zhou and Odom, 2011).

The effect of the angle of the incident light and the thickness of the metal layer on the sensing performance was also studied by evaluating aqueous solutions with different RI. From the generated spectra, both bulk RI sensitivity and FWHM were extracted and the figure of merit (FOM) estimated. As can be observed in Fig. 2c, a higher incident angle promotes an increase in sensitivity and a decrease in FWHM for both thicknesses. Maximum bulk sensitivity and minimum FWHM values were obtained at 70° incident angle of light. A high incident angle increases the possibility to reach higher FOM with these sensors and an enhancement in optical fields due to longer plasmon lifetimes (Zhou and Odom, 2011). Sensitivity values of ≈425 nm RIU^{-1} and 360 nm RIU^{-1} with FWHM values of 12 nm and 15 nm were achieved for 100 nm and 50 nm gold layer thickness, respectively. These behaviors are correlated with the fact that a thin gold layer promotes interaction of plasmons with the underlying substrate with more radiative losses. This could explain a higher FWHM in 50 nm gold layer thickness sensor and lower bulk sensitivity due to a decrease in the intensity of the optical fields (Lee et al., 2016). This behavior is also correlated with the improvement in the sensing performance observed at higher incidence angle. Under these conditions, the interaction between nanostructures increases and the optical energy scattered or their loss as free-space light is reduced, therefore promoting the enhancement of the optical fields (Zhou and Odom, 2011).

The experimental results were corroborated with reflectance spectra and optical field distributions calculated from FDTD simulations. As can be observed in Fig. 3a there is a good agreement between the calculated and the experimental reflectance spectra, with a narrower resonant linewidth for the 100 nm gold thickness film compared to the 50 nm gold film. As previously discussed, this behavior could be related to the interaction of plasmons with the underlying substrate. To evaluate this possibility we analyzed the electric field distributions calculated from FDTD simulations. Fig. 3b and c illustrate the differences in the electric field distributions for a gold thickness layer of 50 and 100 nm, respectively. The interaction of plasmons with the underlying substrate is obvious for the 50 nm gold layer, which causes radiative losses and decreases the intensity of the optical fields with shorter decay lengths. On the other hand, for a 100 nm gold layer a greater intensity and longer decay lengths are observed. These changes

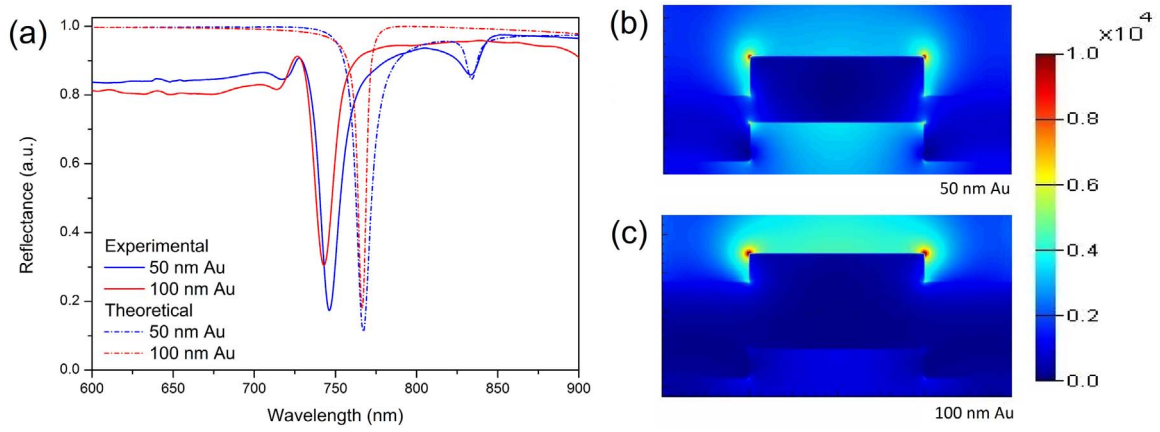

Fig. 3. FDTD Simulations of the proposed sensor. (a) Evaluated and simulated optical reflectance spectra under TM-polarization with a light incident angle of 70° for the two nanostructured plasmonic sensors fabricated. Simulated electric field distribution for the 50 nm (b) and 100 nm (c) gold thickness layer under TM-polarization for a light incidence angle of 70°.

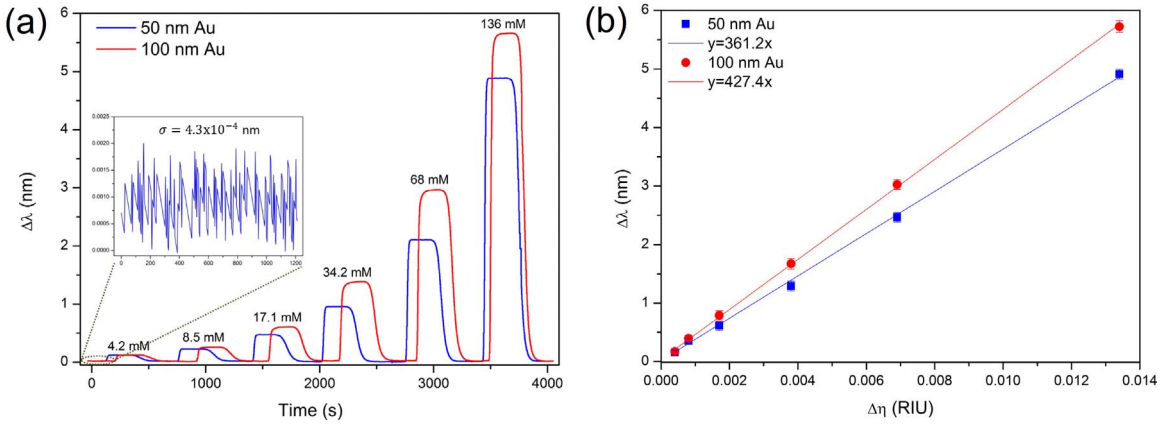

Fig. 4. Sensing performance evaluation. (a) Real-time sensorgrams of different solutions of glycerol for the two gold thickness layer chips fabricated. The insert shows the noise level of the sensor response. (b) Calibration curves and bulk sensitivity determination for the two gold thickness layer chips fabricated at a incidence angle of 70°.

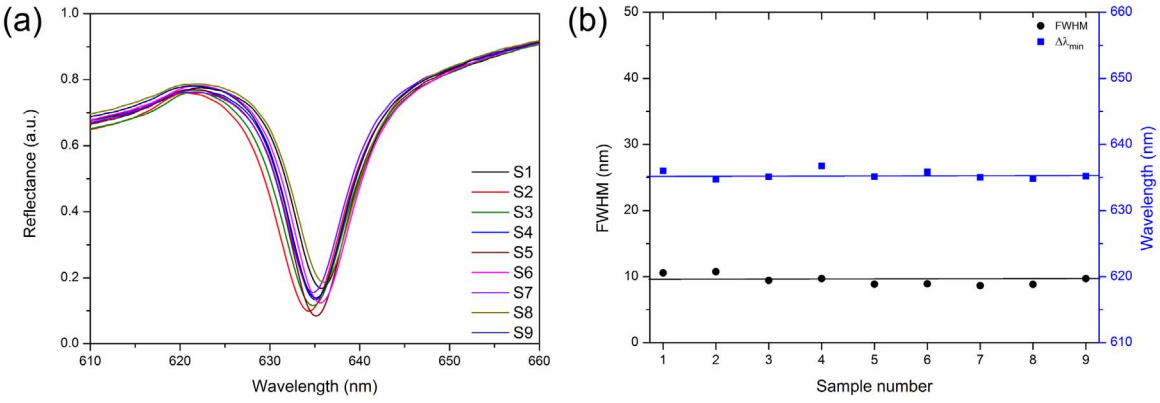

Fig. 5. Reproducibility evaluation of the fabrication process. (a) Reflectance spectra of nine different chips with 100 nm gold thickness obtained in three different fabrication batches. Spectra obtained under TM-polarized light with a fixed incident angle of 70° in air (η=1.00). (b) Resonant wavelengths and FHWM bandwidths of the nine chips. Mean values of 635.3 ± 0.6 nm and 10.1 ± 0.9 nm were obtained, respectively.

in the electric field distribution can be related to the bulk sensitivity improvement we have observed for the 100 nm gold layer. As it has been previously suggested (Mazzotta et al., 2015; Li et al., 2015), an increase in the electric field penetration length to the medium can enhance the bulk sensing performance. Considering the performance of the sensors, a FOM up to 35 RIU^{-1} is achieved with a bulk sensitivity of 425 nm RIU^{-1} (Fig. 4) and a LOD up to $6.3{\cdot}10^{-6}$ RIU for the 100 nm thickness with a 70° light incidence angle. The LOD is near one order or magnitude better than some previously reported engineered nano-slit-based sensors measured under normal light incidence transmittance (Lee et al., 2012, 2015). This configuration increased approximately 20% and 70% the values of the bulk sensitivity and FOM, respectively, compared to reported values obtained also for Blu-ray disc based plasmonic sensors on normal light incidence reflectance measurements (Dou et al., 2012; Guner et al., 2017). In particular, a recently reported SPR imaging (SPRi) platform, based on silver Blu-ray discs and normal light incidence reflectance measurements, exhibited a bulk sensitivity of 356 nm RIU^{-1} and a LOD of $4.12{\cdot}10^{-5}$ RIU, which is

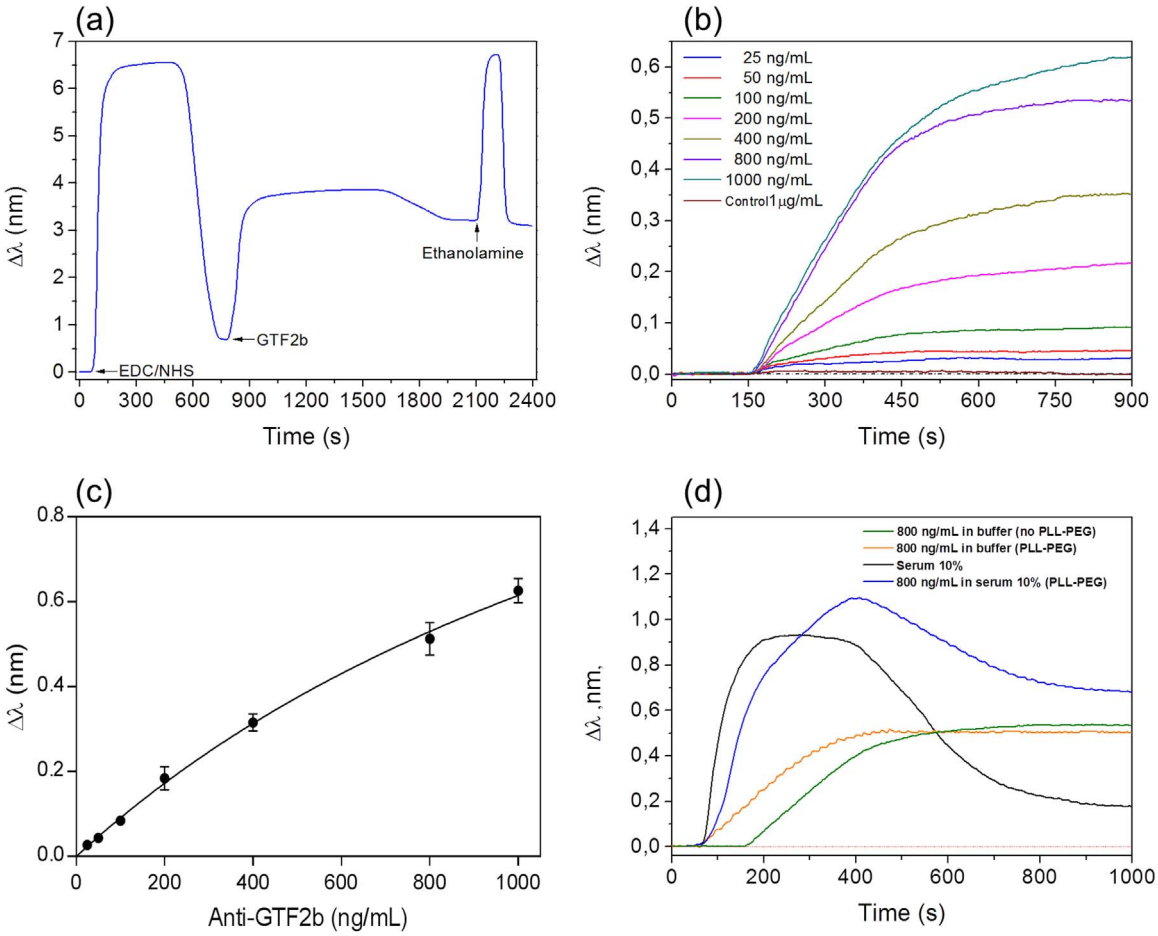

Fig. 6. (a) Real-time sensorgrams showing the covalent immobilization of the protein GTF2b: activation of carboxylic SAM layer with EDC/NHS, attachment of the protein and blocking of unreacted groups; (b) sensorgrams showing the detection of the specific antibody at different concentrations (from 25 to 1000 ng/mL) and control experiment (antibody for protein PIM1); (c) calibration curve for the detection of the anti-GTF2b; (d) Effect of the PLL-PEG blocking step in the detection: green and orange lines shows the detection of antibody (800 ng/mL) without and with PLL-PEG layer, respectively; black line shows the nonspecific binding of 10% diluted serum; blue line shows the detection of antibody (800 ng/mL) in 10% diluted serum. (For interpretation of the references to color in this figure legend, the reader is referred to the web version of this article.)

near one order of magnitude worse than our proposed portable prototype (Guner et al., 2017). Overall, the sensing performance of our device is highly competitive and comparable to the current state of the art in SPR platforms (Lopez et al., 2017; Estevez et al., 2014). Besides, this approach offers simple and reproducible fabrication process. This excellent performance can also be correlated with the good S/N ratio obtained, as can be observed in the real-time sensorgrams (see Fig. 4a) with a noise standard deviation of 4.3×10^{-4} nm. The enhancement in bulk sensitivity and FOM with the increase in the incidence angle confirms that oblique incidence can improve the sensing performance parameters of these metallic nanostructures taking advantage of the generation of Fano resonant modes. The batch to batch fabrication reproducibility is one of the main challenges to demonstrate how to achieve high-throughput nanostructured-based plasmonic biosensors, crucial for a future POC device. The reproducibility of the fabrication process was assessed by recording and analyzing the reflectance spectra of nine samples from three different fabrication batches using the same experimental setup. Analyzing the reflectance spectra presented in Fig. 5a, a mean λ_{SPP}, of 635.3 ± 0.6 nm and FWHM value of 10.1 ± 0.9 nm were obtained. Fig. 5b shows a very low dispersion in both parameters for the nine samples. Overall, both the high-throughput fabrication process of Blu-ray discs at industrial scale, which is completely established, and the simple steps necessary to obtain the final nanoslits (only cleaning and evaporation steps) contribute to the achievement of highly reproducible substrates from batch to batch. The sensor has fixed structural dimensions (height and period of the nanostructures) limiting the tunability of the nanostructures when compared to other approaches (Lee et al., 2015). However, there are opportunities to increase its performance using other plasmonic materials such as graphene (Singh et al., 2015) or exploiting other photonic phenomena (Li et al., 2015). Furthermore, it is a powerful strategy to prototype optical biosensors in small labs, due to its reduced associated costs, which we estimate from 2 to 4 euros per unit, depending on successful microfluidics integration yields. It can also be suitable for testing novel detection strategies and it facilitates large scale fabrication due to industry standards. Finally, it can be easily integrated into microfluidic lab-on-a-disc (Phonchai et al., 2016) to develop comprehensive sensing platforms including sample preparation strategies. Given this simple and cost-effective fabrication process, together with a straightforward integration using inexpensive microfluidics and a detection scheme with extra miniaturization potential, our sensor is a promising candidate for POC platforms.

3.2. Biosensing evaluation with the integrated platform

The potential of the developed integrated plasmonic device for biosensing applications was assessed with a direct assay for the early detection of colorectal cancer based on the detection of specific autoantibodies against GTF2b protein, a suspected TAA related to colorectal cancer. TAAs are overexpressed proteins associated with malignant growth. The detection of the TAAs is highly interesting for early cancer detection. However, these TAAs become even more

relevant since some cancers have demonstrated to be immunogenic, so that they can stimulate the immunoresponse, triggering the generation of specific autoantibodies by the human immunosystem. Therefore, the detection in a patient's blood sample of the generated autoantibodies against these TAAs is even more remarkable as they can be detected at higher concentrations and at very early stages of the disease compared to TAAs (Chen et al., 2014). Most common methodologies used for autoantibodies determination are ELISA or protein microarrays, which provide qualitative or semi-quantitative results based on relative signals compared to reference population (Zaenker and Ziman, 2013; Barderas et al., 2012, 2013; Babel et al., 2009). Therefore the potential for a precise quantification can be highly valued from a diagnostic and a therapy follow-up perspective. Additionally, autoantibodies possess a higher molecular weight, being more suitable for mass-dependent label-free refractometric configurations. This assay was previously developed and characterized with another nanoplasmonic biosensor (Soler et al., 2016). The nanostructured substrate with higher bulk sensitivity (gold film of 100 nm) was modified by forming a SAM with carboxylic acid. Carboxylic groups (CO_2H) were activated by means of the carbodiimide chemistry, which results in a NHS-ester intermediate highly reactive to primary amines (NH_2) present in the GTF2b protein. The chemical procedure is well established and it generates highly stable amide bonds. The immobilization was monitored in real time, as can be seen in Fig. 6a. The detection of the specific antibody associated to this protein shows a good dose-response relation for concentrations of antibody (see Fig. 6b). Given the excellent S/N ratio obtained with the setup and the processing software (~1.1 pm) we were able to achieve a LOD of 3.4 ng/mL (22.6 pM) and a LOQ of 11.4 ng/mL (75.6 pM), respectively (see the calibration curve in Fig. 6c). The values are slightly better than the ones that we previously obtained for the same assay but with gold nanodisks as substrate using an optical setup under prism-coupled TIR (total internal reflection) measurements (Soler et al., 2016). Whereas gold nanodisks offer excellent properties, this new approach provides an even faster and highly reproducible fabrication method and minimizes the optical setup complexity being unnecessary the use of coupling components. In order to preliminary assess also the feasibility of measuring biological samples, an additional blocking step was considered based on the addition of a layer of PLL-PEG, a well-known compound able to minimize nonspecific adsorptions in complex media (Soler et al., 2016). Although the blocking did not completely remove the binding of serum components, resulting in a shift around 0.17 nm for 10% serum (see Fig. 6d, black line) it did not affect the target detection in buffer. As can be seen in Fig. 6d (green and orange lines) similar shift was observed for the same concentration of antibody in buffer before and after blocking, being of 0.51 nm in both cases. When measuring in 10% diluted serum (blue line in Fig. 6d) a total signal of 0.68 nm was observed. This corresponds to the contribution of both the serum ($\Delta\lambda$ around 0.17 nm) and the specific target binding ($\Delta\lambda$ = 0.51 nm). Overall these results reflect the promising performance of this kind of easy-to-fabricate nanostructures, with high potential to implement low cost competitive devices for relevant clinical applications.

4. Conclusions

A simple label-free integrated plasmonic biosensor based on commercial Blu-ray discs has been demonstrated. By exploiting the Fano resonant modes generated in the metallic nanostructures, an enhanced sensitivity has been achieved in reflection measurements under oblique-angle of the incident light compared to normal light incidence measurements. In contrast to other engineered nanoslits based sensors, we took advantage of the high-throughput fabrication process of Blu-ray discs at industrial scale, to achieve highly reproducible substrates from batch to batch. A FOM up to 35 nm^{-1} and a bulk limit of detection (LOD) up to 6.3×10^{-6} RIU were obtained. We have developed a prototype with high potential for integration, including the chip (only 1 cm^2, with the microfluidics pattern incorporated). To evaluate the label-free biosensing capability of the chip we have also demonstrated the real-time detection of specific antibodies for a tumor-associate antigen (GTF2b antigen). A LOD in the pM order was obtained and we observed a promising performance in diluted serum, which reinforces the future applicability of this prototype. Given the simplicity, reproducibility and the low cost of the sensor fabrication process, together with its straightforward integration, the presented device is a promising candidate for the development of competitive POC platforms.

Acknowledgements

GL acknowledges financial support from CONACYT 225362 scholarship. We acknowledge the financial support from COLONTEST project (RETOS-COLABORACIÓN Subprogram, RTC-2014-1518-1) and from PreDICT project (Programa estatal de investigación, desarrollo e innovación orientada a los Retos de la Sociedad, TEC2016-78515-R). The NanoB2A is a consolidated research group (Grup de Recerca) of the Generalitat de Catalunya and has support from the Departament d'Universitats, Recerca i Societat de la Informació de la Generalitat de Catalunya (2014 SGR 624). ICN2 is the recipient of Grant SEV-2013-0295 from the "Severo Ochoa Centers of Excellence" Program of Spanish MINECO. The authors thank Miguel Berenguel Alonso and Prof. Julián Alonso Chamarro from the Group of Sensors and Biosensors (Department of Chemistry, Autonomous University of Barcelona) for their technical support in this work.

References

Acimovic, S.S., Ortega, M.A., Sanz, V., Berthelot, J., Garcia-Cordero, J.L., Renger, J., Maerkl, S.J., Kreuzer, M.P., Quidant, R., 2014. Nano Lett. 14, 2636–2641.
Babel, I., Barderas, R., Diaz-Uriarte, R., Martinez-Torrecuadrada, J.L., Sanchez-Carbayo, M., Casal, J.I., 2009. Mol. Cell Proteom. 8, 2382–2395.
Barderas, R., Babel, I., Diaz-Uriarte, D., Moreno, V., Suarez, A., Bonilla, F., Villar-Vázquez, R., Capellá, G., Casal, J.I., 2012. J. Proteom. 75, 4647–4655.
Barderas, R., Villar-Vázquez, R., Fernández-Aceñero, M.J., Babel, I., Peláez-García, A., Torres, S., Casal, J.I., 2013. Sci. Rep. 3, 2938.
Cappi, G., Spiga, F.M., Moncada, Y., Ferretti, A., Beyeler, M., Bianchessi, M., Decosterd, L., Buclin, T., Guiducci, C., 2015. Anal. Chem. 87, 5278–5285.
Chen, H., Werner, S., Tao, S., Zörnig, I., Brenner, H., 2014. Cancer Lett. 346, 178–187.
Chen, Y., 2015. Microelectron. Eng. 135, 57–72.
Coskun, A.F., Cetin, A.E., Galarreta, B.C., Alvarez, D.A., Altug, H., Ozcan, A., 2014. Sci. Rep. 4, 6789.
Dou, X., Phillips, B.M., Chung, P.Y., Jiang, P., 2012. Opt. Lett. 37, 3681–3683.
Estevez, M.-C., Otte, M.A., Sepulveda, B., Lechuga, L.M., 2014. Anal. Chim. Acta 806, 55–73.
Gartia, M.R., Hsiao, A., Pokhriyal, A., Seo, S., Kulsharova, G., Cunningham, B.T., Bond, T.Z., Liu, G.L., 2013. Adv. Opt. Mater. 1, 68–76.
Guner, H., Ozgur, E., Kokturk, G., Celik, M., Esen, E., Topal, A.E., Ayas, S., Uludag, Y., Elbuken, C., Dana, A., 2017. Sens. Actuators B-Chem. 239, 571–577.
Johnson, P.B., Christy, R.W., 1972. Phys. Rev. B 6, 4370–4379.
Kabashin, A.V., Evans, P., Pastkovsky, S., Hendren, W., Wurtz, G.A., Atkinson, R., Pollard, R., Podolskiy, V.A., Zayats, A.V., 2009. Nat. Mater. 8, 867–871.
Kaplan, B., Guner, H., Senlik, O., Gurel, K., Bayindir, M., Dana, A., 2009. Plasmonics 4, 237–243.
Kooy, N., Mohamed, K., Pin, L.T., Guan, O.S., 2014. Nanoscale Res. Lett. 9, 320.
Lee, K.L., Chen, P.W., Wu, S.H., Huang, J.B., Yang, S.Y., Wei, P.K., 2012. ACS Nano 6, 2931–2939.
Lee, K.L., Huang, J.B., Chang, J.W., Wu, S.H., Wei, P.K., 2015. Sci. Rep. 5, 8547.
Lee, K.L., Chang, C.C., You, M.L., Pan, M.Y., Wei, P.K., 2016. Sci. Rep. 6, 33126.
Li, J., Chen, C., Lagae, L., Van Dorpe, P., 2015. J. Phys. Chem. C 119, 29116–29122.
Lopez, G.A., Estevez, M.-C., Soler, M., Lechuga, L.M., 2017. Nanophotonics 6, 123–136.
Luk'yanchuk, B., Zheludev, N.I., Maier, S.A., Halas, N.J., Nordlander, P., Giessen, H., Chong, C.T., 2010. Nat. Mater. 9, 707–715.
Malic, L., Morton, K., Clime, L., Veres, T., 2013. Lab Chip 13, 798–810.
Mazzotta, F., Johnson, T.W., Dahlin, A.B., Shaver, J., Oh, S.H., Höök, F., 2015. ACS Photonics 2, 256–262.
Offermans, P., Schaafsma, M.C., Rodriguez, S.R., Zhang, Y., Crego-Calama, M., Brongersma, S.H., Gómez Rivas, J., 2011. ACS Nano 5, 5151–5157.
Phonchai, A., Kim, Y., Chantiwas, R., Cho, Y.K., 2016. Lab Chip 16, 3268–3275.
Seo, J.H., Park, J.H., Kim, S.I., Park, B.J., Ma, Z., Choi, J., Ju, B.K., 2014. J. Nanosci. Nanotechnol. 14, 1521–1532.
Shen, Y., Zhou, J., Liu, T., Tao, Y., Jiang, R., Liu, M., Xiao, G., Zhu, J., Zhou, Z., Wang, X., Jin, C., Wang, J., 2013. Nat. Commun. 4, 2381.
Singh, M., Holzinger, M., Tabrizian, M., Winters, S., Berner, N.C., Cosnier, S., Duesberg,

G.S., 2015. J. Am. Chem. Soc. 137, 2800–2803.
Soler, M., Estevez, M.-C., Villar-Vazquez, R., Casal, J.I., Lechuga, L.M., 2016. Anal. Chim. Acta 93, 31–38.
Sreekanth, K.V., Alapan, Y., ElKabbash, M., Wen, A.M., Ilker, E., Hinczewski, M., Gurkan, U.A., Steinmetz, N.F., Strangi, G., 2016. Adv. Opt. Mater. 4, 1767–1772.
Sultanova, N., Kasarova, S., Nikolov, I., 2009. Acta Phys. Pol. A 116, 585–587.
Tokel, O., Inci, F., Demirci, U., 2014. Chem. Rev. 114, 5728–5752.
Xiao, B., Pradhan, S.K., Santiago, K.C., Rutherford, G.N., Pradhan, A.K., 2015. Sci. Rep. 5, 10393.
Zaenker, P., Ziman, M.R., 2013. Cancer Epidemiol. Biomark. Prev. 22, 2161–2181.
Zhou, W., Odom, T.W., 2011. Nat. Nanotechnol. 6, 423–427.